ADVANCED ENERGY MATERIALS
www.advenergymat.de

Check for updates

Atomic-Scale Observation of Off-Centering Rattlers in Filled Skutterudites

Zhen-Hua Ge, Wen-Jie Li, Jing Feng, Fengshan Zheng, Chun-Lin Jia, Di Wu, and Lei Jin**

As one of the most fundamental order parameters, the coordinate order of atoms is a cornerstone in determining the physical and chemical properties of materials. Off-centering shifts of atoms from their centrosymmetric positions, a phenomenon that is closely related to symmetry breaking and structural transitions in crystals, is of key importance in modifying a broad range of fundamental properties, such as ferroelectricity, antiferroelectricity, and piezoelectricity. In thermoelectric materials, which can be used to directly interconvert heat to electricity, off-centering has been proposed in, e.g., lead tellurides, halide perovskites, type I and II clathrates, and filled skutterudites, to be the physical origin of the experimentally measured exceptionally low thermal conductivity, but only indirectly supported from structural refinements and experimental/theoretical vibration mode analyses. In this work, Yb partially filled and Ce fully filled skutterudite is taken as a model system for directly measuring the off-centering shifts of filler atoms, i.e., rattlers, with picometer precision in real space, by means of atomic-resolution negative spherical aberration imaging transmission electron microscopy. This finding allows an in-depth understanding of the relationship between the off-centering and the thermoelectric performance, and the presented methodology here is also applicable to investigate the off-centering phenomena in other functional materials, e.g., ferroelectrics and solar cells.

1. Introduction

Thermoelectric materials are the basis for devices that can directly convert heat to electricity and vice versa, thus holding promises to solve the growing energy crisis nowadays. The performance of a thermoelectric material is evaluated by a dimensionless figure of merit value, $ZT = \sigma S^2 T/\kappa$, where σ, S, T, and κ are electrical conductivity, Seebeck efficiency, absolute temperature (in Kelvin), and thermal conductivity, respectively. An ideal thermoelectric material should be simultaneously a decent charge conductor and a heat insulator, i.e., phonon glass electron crystal (PGEC) as proposed by Slack.[1] Among all state-of-the-art material series explored so far, skutterudites are deemed as decent mid-temperature thermoelectric materials for their unique and regulable crystal structure.

Skutterudite, characterized by the chemical formula MX_3 (M = Co, Rh, or Ir and X = P, As, or Sb), represents an extended group of materials that can be derived from the cobalt arsenide mineral $(Co,Fe,Ni)As_3$ discovered in 1845.[2] Under ambient conditions, skutterudite exhibits a high-symmetrical cubic structure (space group: $Im\bar{3}$, No. 204) with intrinsic inner "cages" formed by corner-sharing MX_6 octahedra, in which a variety of guest atoms can be filled.[2] The atoms in the cages are thus termed as fillers. **Figure 1**a shows the crystal structure of a filled skutterudite in the depiction using 8 × MX_6 corner-sharing octahedra (see the red-and-green ball-and-stick model) in a unit cell as well as the cage-like structure formed by filler-Sb_{12} icosahedra (see cyan cages). In this unit cell, atoms M and X are located at the 8c and 24g Wyckoff positions, respectively, while the filler (F) occupies the 2a position, i.e., the apex and body center of the unit cell lattice. It is therefore common in literature to describe skutterudite as the half of the unit cell, FM_4X_{12}.[2]

The most studied skutterudites for mid-temperature thermoelectric applications are antimony-based alloys, i.e., $(Fe,Co)_4Sb_{12}$, due to the relatively high power factor (σS^2) and comparatively low thermal conductivity that could be achieved deliberately through structural modifications.[3–6] The most effective structural modification in $(Fe,Co)_4Sb_{12}$ is to introduce fillers into the interstitial sites of the cage-like $(Fe,Co)_4Sb_{12}$ lattice. The fillers are usually foreign atoms, for instance, alkali

Z.-H. Ge, W.-J. Li, J. Feng
Faculty of Materials Science and Engineering
Kunming University of Science and Technology
Kunming, Yunnan 650093, China

F. Zheng, C.-L. Jia, L. Jin
Ernst Ruska-Centre for Microscopy and Spectroscopy with Electrons
Forschungszentrum Jülich GmbH
52428 Jülich, Germany
E-mail: l.jin@fz-juelich.de

D. Wu
Key Laboratory for Macromolecular Science of Shaanxi Province
Shaanxi Key Laboratory for Advanced Energy Devices
School of Materials Science and Engineering
Shaanxi Normal University
Xi'an, Shaanxi 710119, China
E-mail: wud@snnu.edu.cn

The ORCID identification number(s) for the author(s) of this article can be found under https://doi.org/10.1002/aenm.202103770.

© 2022 The Authors. Advanced Energy Materials published by Wiley-VCH GmbH. This is an open access article under the terms of the Creative Commons Attribution License, which permits use, distribution and reproduction in any medium, provided the original work is properly cited.

DOI: 10.1002/aenm.202103770

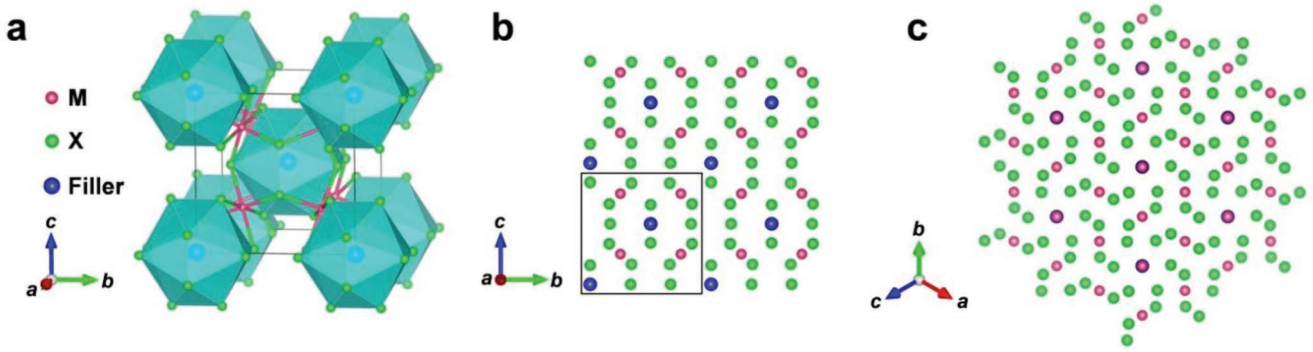

Figure 1. Schematics of the crystal structure of a filled skutterudite FM_4X_{12}. a) Perspective of a unit cell. M atoms: green; X atoms: red; Filler atoms (F): blue. b) Projection of $2 \times 2 \times 2$ unit cells along the <100> axis. The filler atoms are isolated by the skutterudite framework atoms-M_4X_{12}. The selection of unit cell, marked by the black frame, is deliberately shifted away from the filler site as in (a) so that all atoms are fully included in the cell. c) Projection of a filled skutterudite along the <111> direction. Note that the filler atoms align coincidently with M atoms in the viewing direction, resulting in intrinsic difficulties in quantitative characterization of filling atoms.

metals,[7,8] rare earth,[9–12] alkaline earth,[13–15] and the XIII group elements,[16–19] which are believed to enhance phonon scattering and thus lower the thermal conductivity.[2] It is generally accepted that this effect on the thermal transport is attributed to the interaction between heat-carrying phonons and "rattling" fillers. In this regard, filler atoms are assumed to be loosely bonded with surrounding (Fe,Co)-Sb "cages" and thus rattling around individual equilibrium positions with one or more characteristic frequencies (thus called rattlers).[20–22] Hereby, filled skutterudites exhibit the synergetic characteristic of "rigid/stiff framework" and "glass-like vibrator," thus matching quite well with the concept of PGEC in thermoelectrics.[1]

However, the scenario that filler atoms rattle in the (Fe,Co)-Sb cages with fixed frequencies fails to explain the experimentally-measured exceptional low lattice thermal conductivity, as the nondispersive and localized resonant scattering of phonons by fillers only provides a rather limited impedance on the thermal transport. Off-centering of filler atoms was then proposed in skutterudites to explain this discrepancy, and its function could be interpreted as either of the two aspects as follows. In the aspect of lattice strain, off-centered fillers could result in anisotropic distortion on surrounding icosahedral "cages"; while in the aspect of phonon spectrum, the off-center effect broadens the resonant frequency of rattlers thus leading to a flattened lattice vibration spectrum. Chakoumakos et al. reported in 1999 an anomalously large displacement of La off the "cage" center in $LaFe_3CoSb_{12}$ by structural refinement based on neutron diffraction experiments;[23] Goto et al. deduced a thermally activated off-center rattling of Pr ion in the cage of Sb-icosahedron in $PrOs_4Sb_{12}$ from experimental observations of an ultrasonic dispersion of elastic constants; using electron-spin-resonance technique;[24] Garcia et al. found the coexistence of on-center and off-center Yb^{3+} rattles in Ce/Yb double-filled FeP_3;[25] most recently, Fu et al. demonstrated Sn off-centers in its coordination cage, which leads to low-frequency Goldstone-like modes and accounts for the ultralow lattice thermal conductivity in $SnFe_4Sb_{12}$.[26]

In addition, extensive efforts have also been devoted to the detection of fillers in real space, i.e., using advanced atomic-resolution transmission electron microscopy (TEM).[4,27–30] However, direct evidence of positions as well as concentration for filler atoms was rarely reported, in particular at the atomic resolution. Up to now, the widely-used technique for investigation of the off-center behavior of the fillers has been high-angle annular dark-field (HAADF) scanning transmission electron microscopy (STEM), whose image contrast is approximately proportional to Z^2 (Z: atomic number).[31] It is thus commonly called Z-contrast imaging. Therefore, a major challenge for HAADF STEM imaging is that the contrast from filler atoms is typically weak, either below the detection sensitivity or far from being quantitative. This is not only due to the low Z nature of filler atoms, *e.g.*, Ga ($Z = 31$), but also due to the partial occupancy in the cage because of limited solubility.

For example, in <111> zone axes, as shown in Figure 1c, the filler atoms align coincidently with M (e.g., Fe, Co) atoms, resulting in intrinsic difficulties in quantitative measurements of filling atoms (Supporting Information Note 1). While in <100> zone axes, as shown in Figure 1b, the density of the isolated filler atoms (per projected atomic columns) is only half that of the neighboring X atoms (e.g., Sb with $Z = 51$). The density is even lower given the partially filled nature at the positions. These together lead to relatively weak contrast of the filler atoms so that they cannot be distinguished from the surrounding Sb in HAADF STEM imaging (Supporting Information Note 2). Furthermore, the residual aberrations, scanning distortion, etc., are also non-trivial issues in the quantification of the filler atoms. Therefore, techniques that can image the filler atoms with high spatial resolution and high image contrast are crucial to understand the relation between the thermoelectric performance and the behavior of the filler atoms in skutterudites.

In this work, we present a detailed TEM study of both N-type and P-type filled $(Co,Fe)_4Sb_{12}$ thermoelectric alloys employing the negative spherical aberration imaging (NCSI) technique.[32] This technique provides high contrast of both light and heavy atoms and allows ultra-high precision measurement of atom positions.[33–35] We have observed the filler atoms of nominally 20 at.% Yb and fully-filled Ce in skutterudite $(Co,Fe)_4Sb_{12}$ and measured their off-center shifts cage-by-cage with picometer precision on the basis of quantitative high-resolution TEM (HRTEM). The influence of off-center shifts of rattling filler atoms on the thermoelectric properties is further evaluated

© 2022 The Authors. Advanced Energy Materials published by Wiley-VCH GmbH

based on a modified Debye-Callaway model. Our work, for the first time, provides direct evidence on the off-centering rattlers in skutterudites and may shed light on further evidencing off-center atoms in real space for a broad series of thermoelectric materials.

2. Results and Discussion

2.1. Visualization of Filler Atoms Using NCSI

Figure 2a–c shows the atomic-resolution TEM images recorded along the <001> crystal axis under the NCSI conditions for the unfilled Co_4Sb_{12} (pure), nominally 20 at.% Yb filled Co_4Sb_{12} (N-type) and 100 at.% Ce filled $(CoFe_3)Sb_{12}$ (P-type) samples, respectively. In striking contrast to HAADF STEM images (Supporting Information Note 2), all atomic columns, including the low concentration filler Yb (and even Li, see Supporting Information Note 3), are clearly resolved using NCSI (see, e.g., Yb atom marked by the filled arrow in Figure 2b). The visualization is more pronounced from the unit-cell-averaged experimental images (marked by red frames) overlaid on the bottom right corner of Figure 2a–c, alongside the best-fit simulated images marked by green frames (See Supporting Information Note 4 for more details). From the best-fit images, the concentration of filler atoms averaged over the region of measurement is also determined, which is ≈17.5 at.% for Yb and 80 at.% for Ce. The deviation of Ce from its nominal filling stoichiometry indicates a limited solubility of Ce in skutterudites. A similar reduction in solubility has also been reported in $CeFe_4Sb_{12}$[36] and $Ce_{0.1}Co_4Sb_{12}$.[37]

This unique capability of the NCSI technique further allows different configurations of the filler atoms to be studied cage-by-cage in both N- and P-type samples. Four individual configurations of filler atoms, i.e., d1 to d4 (white ellipses in Figure 2b,c) are displayed in Figure 2d as examples. Unlike the P-type sample that has a relatively high filling rate (thus high and homogeneous Ce occupancy shown in Figure 2c), the N-type skutterudite shows local inhomogeneity in the filler's distribution, as directly evidenced by the presence of empty Yb sites (see, e.g., d1 and those marked by open arrows in Figure 2b) with no evident contrast in comparison with those occupied positions indicated by filled arrows (e.g., d2). This finding is consistent with the low filling ratio in the N-type sample.

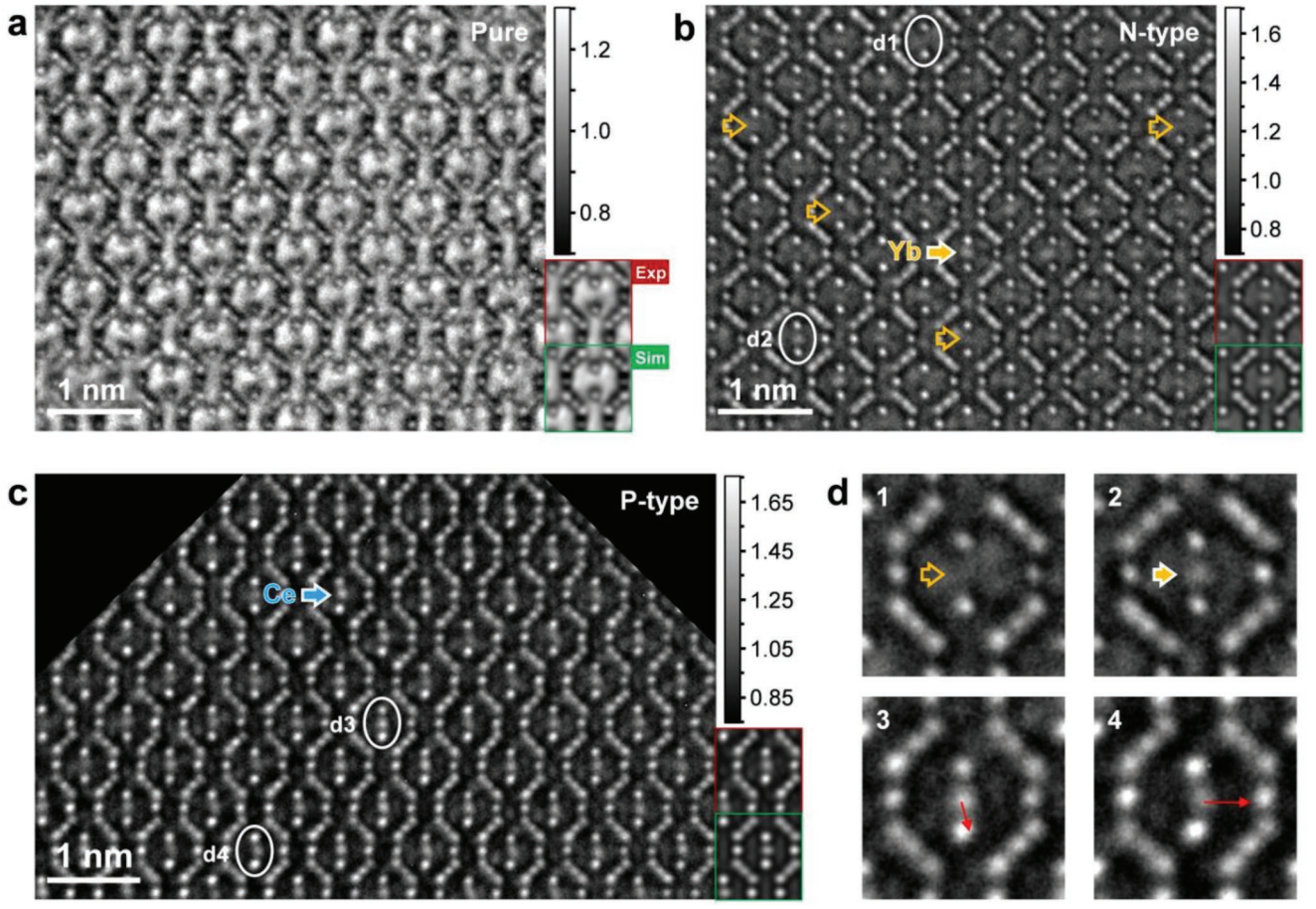

Figure 2. Atomic-resolution TEM images of a) unfilled Co_4Sb_{12} (pure), b) nominally 20 at.% Yb filled Co_4Sb_{12} (N-type) and c) nominally 100 at.% Ce filled $(CoFe_3)Sb_{12}$ (P-type) samples along the <100> crystal axis. Images were recorded under the NCSI conditions. Unit-cell-averaged experimental images and correspondingly the best-fit simulated images are shown in the insets marked by red and green frames, respectively, on the bottom right corner. Images in (a) to (c) are displayed in the same grey scale. d) Magnified images of individual cages, namely d1 to d4, marked by ellipses in (b) and (c), showing four representative configurations of the filler atoms.

© 2022 The Authors. Advanced Energy Materials published by Wiley-VCH GmbH

Noticeably, the filler atoms are found not always to locate the centrosymmetric positions (i.e., cage center) as illustrated in Figure 1a. Instead, they exhibit essential off-center shifts away from the centrosymmetric positions, e.g., in cage d3 and d4, where the off-center shifts of the Ce atoms are marked by red arrows in Figure 2d. Such shifts turn out to be more prominent in the Ce-filled P-type sample, in comparison with the Yb-filled N-type skutterudite.

2.2. Quantitative Measurements of Off-Center Shifts

In order to quantify this off-centering phenomenon, the actual position of each individual intensity maximum in the original image is then determined by fitting 2D Gaussians to its intensity distribution.[38] After proper correction of the effects resulted from imaging imperfections (such as unavoidable sample mistilt from ideal Laue zone directions and residual lens aberrations; so-called imaging artifacts) using quantitative image simulations (Supporting Information Note 4), the measured positions of the intensity maxima in the image represent the atomic positions in the material. Using these positions, the measurement error,[35] defined by the root mean square (rms) of atom-site deviations between the experimental and the best-fit periodic lattice of the Co_4Sb_{12} framework, is better than 7 pm in both horizontal (***x***) and vertical (***y***) directions for all samples used (see Supporting Information Note 5). This measurement error, i.e., precision of atom position measurement, serves as an important basis criterion for subsequent analyses of the filler atoms.

Figure 3 shows the results of off-center shifts in the P-type sample after correction for the known imaging artifacts. In Figure 3a, a larger specimen area is used in order to get better statistics. The off-center shifts of the Ce filler atoms are measured as the position deviation of Ce with respect to the calculated center of the two closest Sb neighbors (in the projected plane), as demonstrated in the inset to Figure 3a. In this inset image, the Ce filler and the Sb atoms are denoted by blue and green filled circles, respectively, and the calculated Sb center by the open circle. In this way, we can provide a simplified solution to evaluate the off-centrosymmetric-position shifts (i.e., shifts from the cage center) by using the relative shift between Ce and the calculated Sb position only. The validity of such measurements is also guaranteed by the fact that the calculated center of Sb is found to be coincident with the cage center (see Supporting Information Note 6). In Figure 3a, the amplitude of the shift vectors can be as large as 60 pm, with an average value (i.e., mean) of 18.6 pm and the spread of shift amplitude (i.e., standard deviation, sd) of 10.0 pm (Figure 3b), further evidencing that the off-center shifts of the Ce filler atoms are prominent.

We further plot the histograms of the shift components in the ***x*** and ***y*** direction as shown in Figure 3c,d, respectively. It is shown that the averaged value of the Ce atom shifts deviates from the cage center by 10.4 and 0.6 pm, with standard deviations of 10.0 and 15.3 pm in the ***x*** and ***y*** directions, respectively, demonstrating that locally (i.e., within the field of view in Figure 3a) the off-center shifts can have directionality. In addition, it should be mentioned that in comparison with the measurement error of <7 pm, both the average value of measured shifts (Figure 3b) and the measured shift spreads (Figure 3c,d) are of statistical significance, confirming the true off-center shifts of the Ce filler atoms in skutterudites.

Similarly, we have also measured the off-center shifts of the Yb filler atoms in the N-type sample. Due to the uneven distribution of Yb in the skutterudite lattice, here we chose positions of the Yb atoms in **Figure 4** with significant image contrast for quantification. The amplitudes of the shift vectors are measured to be between zero and 37 pm with the mean and standard deviation values of 15.4 and 7.5 pm, respectively. Meanwhile, the local directionality of the off-center shifts is not observed.

Since in the P-type skutterudite, the filling ratio of Ce is much higher than that of Yb in the N-type sample and the replacement of Co_4 by $CoFe_3$ may also introduce local inhomogeneity in the Co/Fe atom dispersion as well as local charge redistribution, interactions between neighboring fillers and/or interactions with local Fe/Co dispersion could be responsible for the observed directionality of the off-center shifts. Indeed, it has been reported that in the P-type La and Ce filled Fe_4Sb_{12}, quasi-harmonic coupling between the fillers and the host lattice is a dominant factor to the low thermal conductivity.[20] Thus, the observed directionality may have implication for the breakdown of phonon glass paradigm.

The measurement results are further summarized in **Table 1**, confirming that the off-center shifts are essentially larger in the P-type sample than that in the N-type sample. This, together with the large filling ratio and the local directionality of shifts, is expected to cause stronger influence on the thermoelectric performance in comparison with the effect of the Yb in the N-type skutterudite.

2.3. Rattlers Off-Centering and Lattice Thermal Conductivity

As demonstrated by our NCSI TEM results, partially-filled N-type $Yb_{0.2}Co_4Sb_{12}$ exhibits considerably lower off-centering of the fillers in comparison with fully filled P-type $Ce(CoFe_3)Sb_{12}$ sample, as schematically illustrated in **Figure 5**a. Thermoelectric performance measurements (see Supporting Information Note 8 for details) reveal that $Ce(CoFe_3)Co_{12}$ has a much lower lattice thermal conductivity κ_l than $Yb_{0.2}Co_4Sb_{12}$. In order to evaluate the influence of off-centering on phonon scattering, we have conducted a Debye–Callaway model simulation for pure Co_4Sb_{12}, partially filled $Yb_{0.2}Co_4Sb_{12}$, and fully filled $Ce(CoFe_3)Co_{12}$.

As stated in the introduction part, the off-center effect can be understood in terms of either lattice strain or phonon spectrum (vibration mode) perturbation. To accommodate the Debye-Callaway model, additional factor that off-center rattling (as compared with on-center rattling) imposes on phonon scattering is hereby concluded to be a lattice strain parameter Γ_S, which represents the lattice distortion due to fillers' deviation from the equilibrium center positions. The (on-center) rattling is evaluated via the classic resonant scattering model and the Fe/Co alloying in P-type $Ce(CoFe_3)Co_{12}$ is assumed to introduce mass and strain fluctuations as traditional point defect scattering. The scattering

© 2022 The Authors. Advanced Energy Materials published by Wiley-VCH GmbH

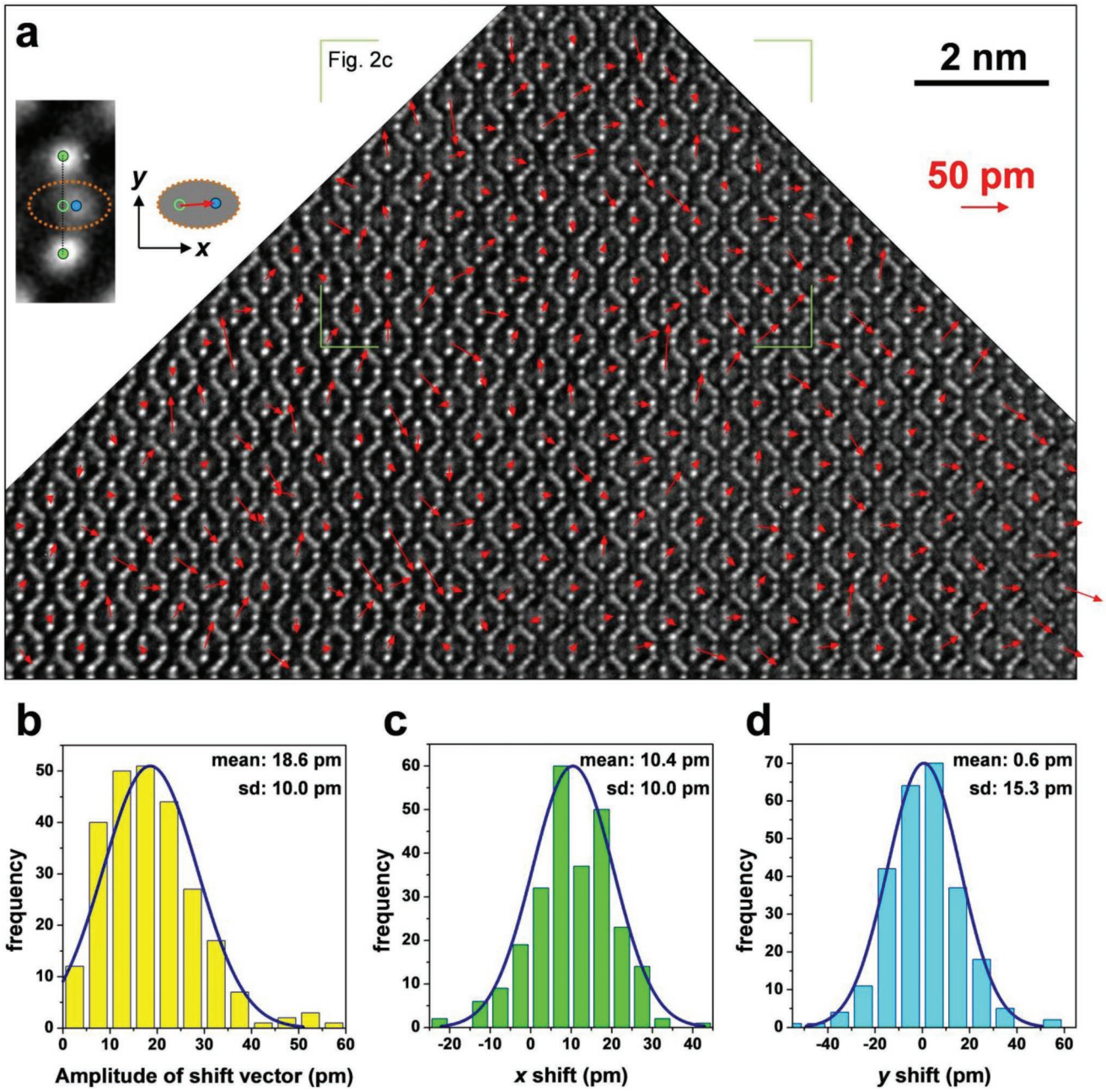

Figure 3. Quantitative measurements of the off-center shifts of the Ce filler atoms in the P-type skutterudite. a) Vector map of the relative shifts of the Ce atoms with respect to the calculated center of two neighboring Sb, overlaid on the experimental NCSI image. The inset in the left to (a) illustrates how to measure the off-center shift. The arrowhead marks the direction and its length represents the amplitude of the shift. The area marked by the green rectangle is also shown in Figure 2c. b) Histogram of the amplitude of the Ce shift vectors in (a). Panels (c) and (d) are histograms of the Ce shifts along the ***x*** and ***y*** directions defined in (a), respectively, showing the local directionality of the off-center shifts, i.e., toward +***x*** direction. The effects of imaging imperfections have been removed.

factors considered in the simulation is then outlined as follows: (i) pure Co_4Sb_3: phonon-phonon scattering + grain boundary scattering; (ii) N-type $Yb_{0.2}Co_4Sb_{12}$: phonon-phonon scattering + grain boundary scattering + resonant scattering + strain scattering; (iii) P-type $Ce(CoFe_3)Co_{12}$: phonon-phonon scattering + grain boundary scattering + Fe/Co alloying scattering + resonant scattering + strain scattering (see Supporting Information Note 9 for details). The final simulated results are shown in Figure 5b.

Spectral lattice thermal conductivity simulation (Supporting Information Note 9) for P-type $Ce(CoFe_3)Co_{12}$ reveals that Fe/Co alloying scattering has minimal effect on phonon scattering due to the very small difference in mass and radius between Fe and Co. It is also shown that resonant scattering dominates

© 2022 The Authors. Advanced Energy Materials published by Wiley-VCH GmbH

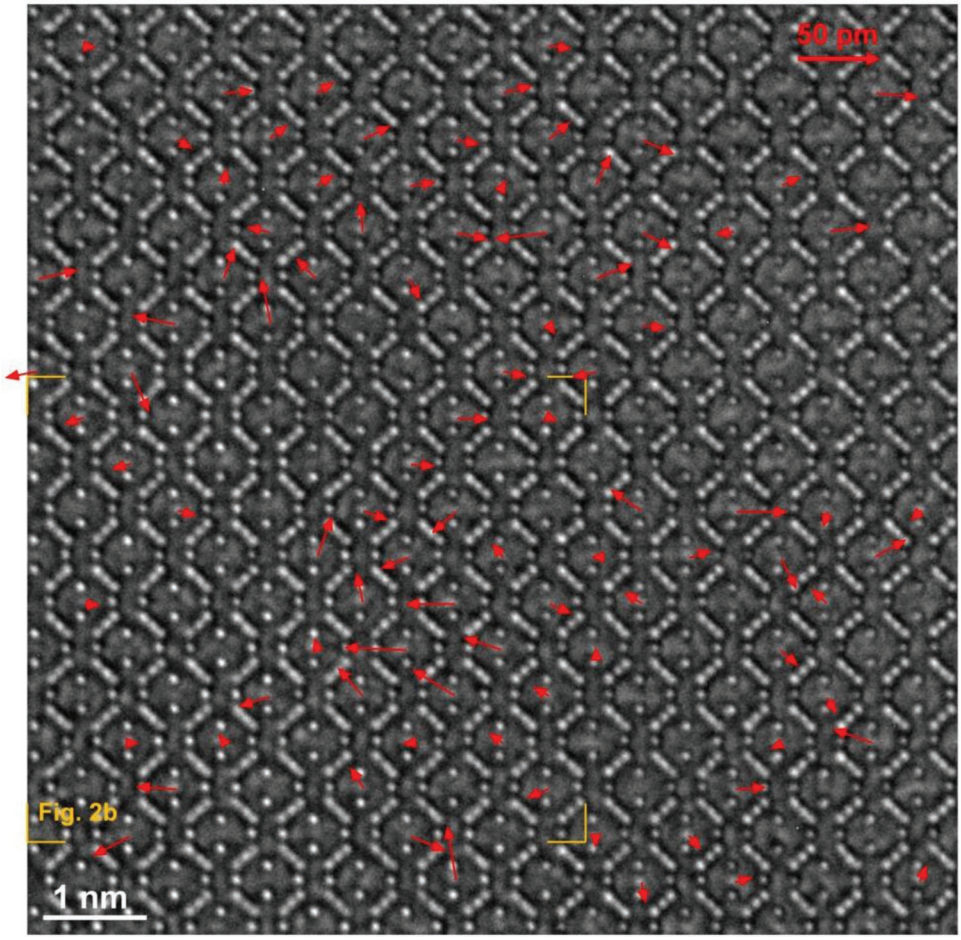

Figure 4. Quantitative measurement of the off-center shifts of the Yb atoms in the N-type skutterudite. a) Vector map of the relative shifts of the Yb atoms with respect to the calculated center of two neighboring Sb atoms, overlaid on the experimental NCSI image. The area marked by the yellow rectangle is also shown in Figure 2b.

at a very localized frequency range only. Direct comparison between N-type $Yb_{0.2}Co_4Sb_{12}$ and P-type $Ce(CoFe_3)Co_{12}$ indicates that i) lattice strain due to the off-center feature of Yb/Ce fillers strongly scatters heat-carrying phonons of a broad frequency range, and ii) the lattice strain ($\Gamma_S \approx 0.55$) in fully filled $Ce(CoFe_3)Co_{12}$ is considerably larger than that ($\Gamma_S \approx 0.15$) in partially filled $Yb_{0.2}Co_4Sb_{12}$. Since the parameter Γ_S directly reflects the extent of lattice (icosahedral "cage") distortion induced by off-center fillers, our simulations agree well with the NCSI TEM results that Ce in fully filled $Ce(CoFe_3)Co_{12}$ exhibits a relatively larger statistic off-center shift. The fact that off-center rattling (on-center rattling + lattice distortion) could scatter heat-carrying phonons for a much broader frequency range than on-center rattling that only scatter phonons at a localized one thus provides an alternative clue to help understand the ultralow lattice thermal conductivity in filled skutterudites.

Table 1. The measured filling ratio, maximal filler shift, amplitude of shift vector, off-center shifts *x* and *y* for the N-type $Yb_{0.2}Co_4Sb_{12}$ and P-type $Ce(CoFe_3)Sb_{12}$ samples. The values in the brackets are standard deviations.

	Measured filling ratio	Maximal filler shift [pm]	Amplitude of shift vector [pm]	Off-center shift *x* [pm]	Off-center shift *y* [pm]
N-type	17.5%	37 pm	15.4 (7.5)	1.1 (14.4)	1.7 (9.2)
P-type	80%	60 pm	18.6 (10.0)	10.4 (10.0)	0.6 (15.3)

3. Conclusion

In summary, using atomic-resolution NCSI TEM, the filler (rattling) atoms in Sb-based skutterudite $(Co,Fe)_4Sb_{12}$, including both 20 at.% partially filled Yb and fully filled Ce, are atomically resolved with high contrast in real space. Based on quantitative image simulations, the off-center shifts of filler atoms are unambiguously confirmed and directly measured cage-by-cage with picometer precision. The off-centering of Yb, Ce fillers is believed to cause considerable lattice strain in (Co,Fe)-Sb "cages" and results in a distinct phonon spectrum compared to on-centering fillers based on the evaluation using a modified Debye–Callaway model. Our findings in this work shed light on further evidence for atom off-center shifts in real space for a broad series of material systems.

© 2022 The Authors. Advanced Energy Materials published by Wiley-VCH GmbH

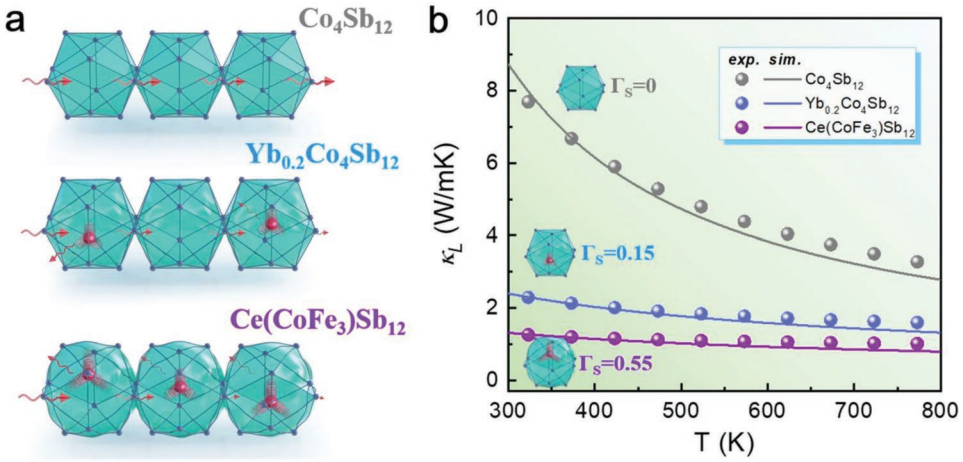

Figure 5. a) Schematics of lattice strain induced by off-centering rattlers. b) Lattice thermal conductivity of unfilled Co_4Sb_{12}, Yb partially filled $Yb_{0.2}Co_4Sb_{12}$ and Ce fully filled $Ce(CoFe_3)Sb_{12}$ skutterudite samples.

4. Experimental Section

Materials Synthesis: Co_4Sb_{12} (pure), $Yb_{0.2}Co_4Sb_{12}$ (N-type), and $Ce(CoFe_3)Sb_{12}$ (P-type) skutterudite samples were synthesized by vacuum melting and spark plasma sintering (SPS). The raw materials consisted of high-purity Co (power, 99.99%), Sb (power, 99.99%), Ce (power, 99.99%), and Yb (power, 99.99%). The mixtures were first loaded in double quartz tubes at ≈10^{-4} Pa, which could prevent samples from exploding in the tube during the cooling process. Then, the mixtures were heated to 1273 K and maintained for 10 h. After soaking for 10 h, the tubes were brought to room temperature in 10 h. The obtained ingots were crushed and ground into powder by high-energy ball milling at 800 rpm for 10 min. The powder was loaded into a φ20 mm graphite die and consolidated using an SPS system (SPS-211Lx, Japan) at 923 K under a pressure of 50 MPa for 5 min.

Phase Structure Characterization: The phase structure of the samples was determined using X-ray diffraction (XRD) on a Bruker D8 diffractometer with monochromated Cu $K_{\alpha 1}$ radiation (wavelength = 1.541 Å). The XRD scan ranges from 10 to 70° with a speed of 10° min^{-1} and a step size of 0.02°.

Thermoelectric Properties Measurement and Analysis: The electrical conductivity (σ) and Seebeck coefficient (S) of all samples were measured (ZEM-3, ULVAC-RIKO, Japan) in a rarefied helium atmosphere. The thermal diffusivity (D) of all bulk samples was measured by laser flash method (LFA 457, NETZSCH LFA, Germany) in an Ar atmosphere using Cowan model plus pulse correction, and the total thermal conductivity (κ) was calculated on the basis of $\kappa = DC_P\rho$ (C_P: heat capacity and ρ: density). The Archimedes method was used to measure the density ρ. Finally, the experimentally determined uncertainty of the Figure of merit ZT value is ≈15–20%. The approximated lattice thermal conductivity κ_l and fitting details with Debye–Callaway model can be found in Supporting Information Note 9.

TEM Sample Preparation: Specimens for transmission electron microscopy investigations were prepared from the as-synthesized bulk polycrystals by standard procedures including cutting, mechanical grinding, dimpling, and polishing. The final thinning of the specimens was carried out using 5 kV Ar-ion milling in a GATAN Precision Ion Polishing System II, followed by a cleaning process at 1 kV in order to remove damaged layers that may be introduced during the previous step. Specimens for scanning transmission electron microscopy energy dispersive X-ray spectroscopy (Supporting Information Note 1) were prepared using focused ion beam milling with Ga ions in an FEI Helios NanoLab 460F1 dual beam system.[39]

Transmission Electron Microscopy: Electron microscopy at atomic resolution was performed using the negative spherical aberration (C_S) imaging technique on an image C_S-corrected FEI Titan 80–300 transmission electron microscope working at an accelerating voltage of 300 kV and a Rayleigh resolution of 80 pm.[40] The NCSI technique yields strong image contrast that is localized as much as possible on the respective atomic columns, allowing ultra-high precision measurement of atom positions on the basis of computer-based image analysis.[33–35] Residual lens aberrations of the microscope were measured by the Zemlin tableau method and minimized rightly before image acquisition. The images were recorded using a GATAN UltraScan 1000 2k × 2k charge-coupled device camera at a sampling rate of 9 pm per pixel. Atomic-resolution high-angle annular dark-field scanning transmission microscopy imaging and corresponding energy dispersive X-ray spectroscopic (EDXS) elemental mapping displayed in the Supporting Information Note 1 were carried out at 200 kV in an FEI Titan G^2 80–200 ChemiSTEM microscope equipped with a high-brightness field emission gun, a probe C_S corrector, and a super-X EDXS system.[41] The incident electron beam convergence semi-angle for HAADF STEM imaging was ≈25 mrad, while the collection semi-angle was 70–200 mrad. EDXS were collected and analyzed using Bruker ESPRIT and Thermo Scientific Velox software.

Image Simulations and Quantification: Multislice image simulations for both NCSI and HAADF STEM were carried out using Dr. Probe software.[42] Atomic models used in the simulations were modified using home-made scripts on the basis of ICSD-185372[37] and were visualized using VESTA software.[43] Quantitative comparison between experimental and simulated NCSI images was performed on the absolute contrast scale[34,44,45] by taking into account the effect of camera modulation-transfer function, specimen absorption, and image spread resulting mainly from thermal-magnetic field noise (Johnson noise)[46] in the optical path of a microscope using an iterative and semi-automatic approach with the assistance of home-made software package. Prior to comparison, the mean intensity of each image was normalized to a dimensionless value of 1, and the corresponding standard deviation of intensity spread represented the image contrast.[34] Simulation parameters for the best-fit NCSI images are listed in Table S1 (Supporting Information).

[Further details of the crystal structure investigation(s) may be obtained from the Fachinformationszentrum Karlsruhe, 76 344 Eggenstein-Leopoldshafen (Germany), on quoting the depository number ICSD-185372].

Supporting Information

Supporting Information is available from the Wiley Online Library or from the author.

© 2022 The Authors. Advanced Energy Materials published by Wiley-VCH GmbH

Acknowledgements

This work was financially supported by the National Natural Science Foundation of China (Grant No. 52162029), Natural Science Foundation of Shaanxi Province (grant No. 2021JM-201), Academician (Expert) Workstation of Yunnan Province Program (Grant No. 202005AF150010), Yunnan Provincial Natural Science Key Fund (Grant No. 202101AS070015). W.D. thanks the support of Shaanxi Sanqin Scholars Innovation Team. The authors thank Juri Barthel (RWTH Aachen University and Forschungszentrum Jülich GmbH) for sharing the home-made software package for semi-automatic quantitative image comparison.

Open access funding enabled and organized by Projekt DEAL.

Conflict of Interest

The authors declare no conflict of interest.

Data Availability Statement

The data that support the findings of this study are available from the corresponding author upon reasonable request.

Keywords

electron microscopy, filled skutterudites, NCSI, off-centering, rattle, thermoelectrics

Received: December 2, 2021
Revised: February 10, 2022
Published online: February 27, 2022

[1] G. A. Slack, in *CRC handbook of thermoelectrics*, (Ed: D. M. Rowe), CRC Press LLC, Boca Raton, Florida, USA, **1995**, Ch. 34.
[2] M. Rull-Bravo, A. Moure, J. F. Fernández, M. Martín-González, *RSC Adv.* **2015**, *5*, 41653.
[3] B. C. Sales, D. Mandrus, R. K. Williams, *Science* **1996**, *272*, 1325.
[4] X. Shi, J. Yang, J. R. Salvador, M. Chi, J. Y. Cho, H. Wang, S. Bai, J. Yang, W. Zhang, L. Chen, *J. Am. Chem. Soc.* **2011**, *133*, 7837.
[5] Y. Tang, Z. M. Gibbs, L. A. Agapito, G. Li, H. S. Kim, M. B. Nardelli, S. Curtarolo, G. J. Snyder, *Nat. Mater.* **2015**, *14*, 1223.
[6] W. Zhao, Z. Liu, Z. Sun, Q. Zhang, P. Wei, X. Mu, H. Zhou, C. Li, S. Ma, D. He, P. Ji, W. Zhu, X. Nie, X. Su, X. Tang, B. Shen, X. Dong, J. Yang, Y. Liu, J. Shi, *Nature* **2017**, *549*, 247.
[7] Y. Z. Pei, L. D. Chen, W. Zhang, X. Shi, S. Q. Bai, X. Y. Zhao, Z. G. Mei, X. Y. Li, *Appl. Phys. Lett.* **2006**, *89*, 221107.
[8] Y. Z. Pei, J. Yang, L. D. Chen, W. Zhang, J. R. Salvador, J. Yang, *Appl. Phys. Lett.* **2009**, *95*, 042101.
[9] D. T. Morelli, G. P. Meisner, B. Chen, S. Hu, C. Uher, *Phys. Rev. B* **1997**, *56*, 7376.
[10] G. S. Nolas, J. L. Cohn, G. A. Slack, *Phys. Rev. B* **1998**, *58*, 164.
[11] G. S. Nolas, M. Kaeser, R. T. L. IV, T. M. Tritt, *Appl. Phys. Lett.* **2000**, *77*, 1855.
[12] A. Grytsiv, P. Rogl, S. Berger, C. Paul, E. Bauer, C. Godart, B. Ni, M. M. Abd-Elmeguid, A. Saccone, R. Ferro, D. Kaczorowski, *Phys. Rev. B* **2002**, *66*, 094411.
[13] L. D. Chen, T. Kawahara, X. F. Tang, T. Goto, T. Hirai, J. S. Dyck, W. Chen, C. Uher, *J. Appl. Phys.* **2001**, *90*, 1864.
[14] M. Puyet, B. Lenoir, A. Dauscher, M. Dehmas, C. Stiewe, E. Müller, *J. Appl. Phys.* **2004**, *95*, 4852.
[15] X. Y. Zhao, X. Shi, L. D. Chen, W. Q. Zhang, W. B. Zhang, Y. Z. Pei, *J. Appl. Phys.* **2006**, *99*, 053711.
[16] G. S. Nolas, H. Takizawa, T. Endo, H. Sellinschegg, D. C. Johnson, *Appl. Phys. Lett.* **2000**, *77*, 52.
[17] B. C. Sales, B. C. Chakoumakos, D. Mandrus, *Phys. Rev. B* **2000**, *61*, 2475.
[18] G. S. Nolas, J. Yang, H. Takizawa, *Appl. Phys. Lett.* **2004**, *84*, 5210.
[19] T. He, J. Chen, H. D. Rosenfeld, M. A. Subramanian, *Chem. Mater.* **2006**, *18*, 759.
[20] M. M. Koza, M. R. Johnson, R. Viennois, H. Mutka, L. Girard, D. Ravot, *Nat. Mater.* **2008**, *7*, 805.
[21] R. Viennois, L. Girard, D. Ravot, H. Mutka, M. Koza, F. Terki, S. Charar, J. C. Tedenac, *Phys. B* **2004**, *350*, E403.
[22] J. L. Feldman, D. J. Singh, I. I. Mazin, D. Mandrus, B. C. Sales, *Phys. Rev. B* **2000**, *61*, R9209.
[23] B. C. Chakoumakos, B. C. Sales, D. Mandrus, V. Keppens, *Acta Cryst.* **1999**, *B55*, 341.
[24] T. Goto, Y. Nemoto, K. Sakai, T. Yamaguchi, M. Akatsu, T. Yanagisawa, H. Hazama, H. S. K. Onuki, H. Sato, *Phys. Rev. B* **2004**, *69*, 180511.
[25] F. A. Garcia, D. J. Garcia, M. A. Avila, J. M. Vargas, P. G. Pagliuso, C. Rettori, M. C. G. PasseggiJr., S. B. Oseroff, P. Schlottmann, B. Alascio, Z. Fisk, *Phys. Rev. B* **2009**, *80*, 052401.
[26] Y. Fu, X. He, L. Zhang, D. J. Singh, *Phys. Rev. B* **2018**, *97*, 024301.
[27] Y. Qiu, J. Xing, X. Gao, L. Xi, X. Shi, H. Gu, L. Chen, *J. Mater. Chem. A* **2014**, *2*, 10952.
[28] X. Shi, J. Yang, L. Wu, J. R. Salvador, C. Zhang, W. L. Villaire, D. Haddad, J. Yang, Y. Zhu, Q. Li, *Sci. Rep.* **2015**, *5*, 14641.
[29] Y. Wang, J. Mao, Q. Jie, B. Ge, Z. Ren, *Appl. Phys. Lett.* **2017**, *110*, 163901.
[30] Z. Liu, X. Meng, D. Qin, B. Cui, H. Wu, Y. Zhang, S. J. Pennycook, W. Cai, J. Sui, *J. Mater. Chem. C* **2019**, *7*, 13622.
[31] S. J. Pennycook, L. A. Boatner, *Nature* **1988**, *336*, 565.
[32] C. L. Jia, M. Lentzen, K. Urban, *Science* **2003**, *299*, 870.
[33] C. L. Jia, L. Houben, A. Thust, J. Barthel, *Ultramicroscopy* **2010**, *110*, 500.
[34] C. L. Jia, S. B. Mi, J. Barthel, D. W. Wang, R. E. Dunin-Borkowski, K. W. Urban, A. Thust, *Nat. Mater.* **2014**, *13*, 1044.
[35] C. L. Jia, L. Jin, Y. H. Chen, K. W. Urban, H. Wang, *Ultramicroscopy* **2018**, *192*, 57.
[36] Y. G. Yan, W. Wong-Ng, L. Li, I. Levin, J. A. Kaduk, M. R. Suchomel, X. Sun, G. J. Tan, X. F. Tang, *J. Solid State Chem.* **2014**, *218*, 221.
[37] J. L. Mi, M. Christensen, E. Nishibori, B. B. Iversen, *Phys. Rev. B* **2011**, *84*, 064114.
[38] L. Houben, iMtools general purpose multi platform image procession tools, https://er-c.org/index.php/software/stem-data-analysis/imtools/, (accessed: November 2021).
[39] Ernst Ruska-Centre for Microscopy and Spectroscopy with Electrons, *J. Large-Scale Res. Facil.* **2016**, *2*, A59.
[40] Ernst Ruska-Centre for Microscopy and Spectroscopy with Electrons, *J. Large-Scale Res. Facil.* **2016**, *2*, A41.
[41] Ernst Ruska-Centre for Microscopy and Spectroscopy with Electrons, *J. Large-Scale Res. Facil.* **2016**, *2*, A43.
[42] J. Barthel, *Ultramicroscopy* **2018**, *193*, 1.
[43] K. Momma, F. Izumi, *J. Appl. Crystallography* **2011**, *44*, 1272.
[44] C. L. Jia, J. Barthel, F. Gunkel, R. Dittmann, S. Hoffmann-Eifert, L. Houben, M. Lentzen, A. Thust, *Microsc. Microanal.* **2013**, *19*, 310.
[45] L. Jin, J. Barthel, C. L. Jia, K. W. Urban, *Ultramicroscopy* **2017**, *176*, 99.
[46] S. Uhlemann, H. Müller, P. Hartel, J. Zach, M. Haider, *Phys. Rev. Lett.* **2013**, *111*, 046101.

© 2022 The Authors. Advanced Energy Materials published by Wiley-VCH GmbH